ISSN 0915-633X

NATIONAL INSTITUTE FOR FUSION SCIENCE

Development and Simulation of RF Components for High Power Millimeter Wave Gyrotrons

M. Pereyaslavets, M. Sato, T. Shimozuma, Y. Takita, H. Idei, S. Kubo, K. Ohkubo and K. Hayashi

(Received - Oct. 23, 1996)

NIFS-464 Nov. 1996

RESEARCH REPORT
NIFS Series

NAGOYA, JAPAN

Development and simulation of RF components for high power millimeter wave gyrotrons

M. Pereyaslavets, M. Sato, T. Shimozuma, Y. Takita, H. Idei, S. Kubo, K. Ohkubo and K. Hayashi*

National Institute for Fusion Science, Furo-cho, Chikusa-ku, Nagoya 464-01, Japan
*Energy and Mechanical Laboratories, Toshiba Corporation, 4-1 Ukishima-cho, Kawasaki-ku, Kawasaki 210 Japan

Abstract

To test gyrotron RF components, efficient low-power generators for rotating high-order modes of high purity are necessary. Designs of generators for the $TE_{15,3}$ mode at 84 GHz and for the $TE_{31,8}$ mode at 168 GHz are presented and some preliminary test results are discussed. In addition, Toshiba gyrotron cavities at 168 GHz were analyzed for leakage of RF power in the beam tunnel. To decrease RF power leakage, the declination angle of the cut-off cavity cross section has to be decreased. A $TE_{15,3}$ waveguide nonlinear uptaper is analyzed at 84 GHz as well as 168 GHz uptapers. Since the calculated conversion losses are slightly higher than designed value, an optimization of those uptapers may be required.

Key words: gyrotron cavity, mode generator, mode conversion, waveguide uptaper

1. Introduction

RF components of gyrotrons: the cavity, the Vlasov launcher with the corresponding mirrors and the output window are extremely important at high-power levels, especially when the CW operation of a gyrotron is required. Those components should be tested by a low power RF field before their installation in a gyrotron to diminish power losses and to verify the results from their design and manufacture. Therefore, low power mode generators are necessary in addition to appropriate computer simulation tools. This paper presents some designs of low power gyrotron-type mode generators as well as analysis of RF power leakage in the beam tunnel for $TE_{22,6}$ and $TE_{31,8}$ mode cavities at 168 GHz. In addition, mode conversion was analyzed for $TE_{15,3}$ waveguide up-tapers at 84 GHz. We have elaborated some practical recommendations improving existing designs.

2. Design of low- power mode generators

The design of mode generators used in this paper is based on the method described in Alexandrov et al. (1992, 1995), Braz et al. (1995,1996) and Pereyaslavets et al. (1997). The hollow cylindrical cavities are installed in the high power gyrotrons considered in this paper. However, coaxial cavities were employed for low power mode generators, since their mode spectrum is more sparse. In such a way, to generate a pure high-order rotating circular waveguide mode, a coaxial cylindrical cavity with perforated wall is illuminated by a low power Gaussian beam which is focused by a quasi-optical mirror (Fig. 2.1).

The design of the coaxial cylindrical cavity is described in detail by Alexandrov et al. (1995). The inner conductor is required to reduce mode competition and to increase the purity of the desired mode.

This paper considers an advanced design of the quasi-optical mirror and of the cavity wall perforation, leading to an efficiency enhancement and to a significantly higher mode purity. Mode generators for the $TE_{15,3}$ mode at 84 GHz and for the $TE_{31,8}$ mode at 168 GHz were designed. Further we describe briefly main steps of the design procedure.

First, the eigenfrequency corresponding to a root of a Bessel function of the desired mode is compared with other hollow waveguide modes and the nearest competing modes are determined. Following Alexandrorv et al. (1995), the ratio of the diameters of the external cylinder and the inner rod is selected to decrease the mode competition with the desired mode.

Second, a coaxial gyrotron-type cavity is designed for the desired low power mode. Its quality factor must be large enough to allow mode selection with a desired mode purity. Usually the quality factor is approximately ten times the inverse relative separation of competing modes eigenfrequencies. The final quality factor Q_f is composed from the cavity quality factor Q_g, the perforated holes quality factor Q_h and the ohmic quality factor Q_{ohm} as

$$\frac{1}{Q_f} = \frac{1}{Q_g} + \frac{1}{Q_h} + \frac{1}{Q_{ohm}} \qquad (1)$$

The maximal efficiency is achieved if the perforated holes quality factor is equal to (or slightly greater than) the cavity quality factor

$$Q_g = Q_h \ . \tag{2}$$

One should take into account that the real resonant frequency is always lower than the designed one, since perforated holes and ohmic losses in the real cavity walls decrease the computed resonant frequency. One could estimate such frequency shift from the expected values of the quality factors for perforated holes and ohmic losses:

$$\frac{\Delta f}{f} = \frac{\tan^{-1}\left(\sqrt{\pi/(2Q)}\right)}{\pi} \approx \sqrt{\frac{1}{2\pi Q}} \ . \tag{3}$$

Third, the quasi-optical mirror must be designed for a given Gaussian beam illumination or, alternatively, the Gaussian beam parameters can be determined to achieve the maximal efficiency. Such a procedure is described in Pereyaslavets et al. (1997), where the formulas of Vlasov and Shapiro (1989) and Denisov et al. (1992) were improved. According to this method, the plane phase front of the Gaussian beam must be replaced by a point source, taking into account the phase front curvature of the incident Gaussian beam. Then the shape of the mirror is derived by means of equal optical path length. The rays have to be reflected in such a way that they form a circular caustic representing the desired rotating TE mode. The reflector is designed by the requirement of equal optical path length between the plane phase front of the incident beam and the phase front of the caustic, i.e., its involute. One could count the ray path from a reference plane of the phase front to the point of the ray emergence from the mode caustic inside the cavity and plus the distance along the caustic to a reference point.
Alternatively, a procedure of Wada et al. (1988) solving a differential equation could be employed for the mirror design.

Fourth, the designed quasi-optical mirror should be analyzed to determine the mode excitation efficiency and to correct mirror design parameters like the location of the mirror and the waist of the Gaussian beam. Following Pereyaslavets et al. (1997), a computer code was developed using the current distribution method (Silver, 1984), here the currents on a mirror are assumed to be proportional to the fields of an incident wave. The field reflected by the mirror is computed at the position of the internal boundary of the coaxial cavity. The simulation does not take into account a reflection from the metallic cavity surface. To calculate how much power is coupled by the mirror to the desired rotating mode, i.e., to analyze a mirror design, the magnetic field on the cavity boundary is expanded in a Fourier series of the azimuthal angle. The Fourier coefficients give the relative powers of various TE_{mn} modes in the field exciting the cavity. One is primary interested in the power of the desired mode and in powers of neighboring competing modes.

Fifth, the perforation of the cavity wall is designed. Let us determine the optimum perforation parameters, i.e., the number and diameter of the holes and the distances

between them, following Pereyaslavets (1997). The power balance must be satisfied for the mode converter. This means the P_{in} power coupled through the perforated wall must be equal to the power P_{out} radiated through the axially open end of the cavity. The mutual interaction between the holes is to be taken into account for our frequency range, so the diffraction theory has to be used to calculate the coupling through the holes.

A thin semi-transparent surface with boundary conditions of coupling is an approximation, used for scattering on a perforated plate (i.e., the cavity wall). The real parameter ρ_1 characterizes the coupling through the perforated wall. The transmission through a semi-transparent plane is expressed in terms of ρ_1 as:

$$|T^2| = \frac{4\rho_1^2}{1+4\rho_1^2} \quad . \tag{4}$$

The simple approximation is very useful for synthesis of a mode generator with perforated walls (Pereyaslavets 1985). Rigorous numerical analysis methods, for example by Roberts et al. (1994), require significant CPU time. On the cavity wall ($r=a$) the boundary condition can be written in the form:

$$E_\varphi^+(r=a,\varphi) = E_\varphi^-(r=a,\varphi) \quad , \tag{5}$$

$$E_\varphi^-(r=a,\varphi) = i\,\rho_1 \left[H_z^+(r=a,\varphi) - H_z^-(r=a,\varphi)\right] \quad . \tag{6}$$

Here, the '+' and '-' superscripts denote the fields inside and outside the cavity respectively. Since the magnitude of the H_z^+ field inside the cavity is significantly greater than H_z^-, one can neglect H_z^- in eq. (6) and derive ρ_1 as a function of φ:

$$\rho_1(\varphi) = \left|\frac{E_\varphi^-(r=a,\varphi)}{H_z^+(r=a,\varphi)}\right| \quad . \tag{7}$$

In fact, ρ_1 is to be real and we supposed in eq. (7) that the absolute value gives us a good approximation. Equation (7) determines how the perforation is to be tapered along the cavity wall. Let us also assume the illuminating field E_φ^- contains mainly the desired TE_{mn} mode and can be represented on the cavity boundary in the main order of magnitude as:

$$E_\varphi^-(r=a,\varphi) \;=\; A_m \quad S(\varphi) \quad e^{im\varphi} \quad , \tag{8}$$

where $S(\varphi)$ is a real, slowly changing function and

$$\int_0^{2\pi} |S(\varphi)|^2 \, d\varphi \;=\; 1 \;. \tag{9}$$

So, we derive the illuminating field outside the cavity as

$$E_\varphi^-(\mathrm{r},\,\varphi) = A_m \;\; S(\varphi)\,\frac{H_m^{(1)'}(kr)}{H_m^{(1)'}(ka)} \;\; e^{im\varphi}, \tag{10}$$

$$H_z^-(r,\varphi) = -\frac{i}{k} \;\; A_m \;\; S(\varphi)\,\frac{H_m^{(1)}(kr)}{H_m^{(1)'}(ka)} \;\; e^{im\varphi} \;. \tag{11}$$

Here, $H_m^{(1)}(kr)$ and $H_m^{(1)'}(ka)$ are the Hankel function and its derivation. Using eqs. (10) and (11) the incident power of the illuminating field is estimated as:

$$P_{in} = \frac{c}{4\pi} a \,\mathrm{Re} \int_0^L \int_{\varphi_1}^{\varphi_2} \left\{ \vec{E}_\varphi^-(r=a,\varphi) \left[\vec{H}_z^-(r=a,\varphi) \right]^* \right\} d\varphi \; dz = \left| A_m \right|^2 D \;, \tag{12}$$

where

$$D = \frac{c}{2}\frac{aL}{k}\,\mathrm{Re}\left[i \frac{H_m^{(1)'}(ka)}{H_m^{(1)}(ka)} \right] \;, \tag{13}$$

and L is the cavity length along the z axis. The φ integration in eq. (12) is performed over the perforated cavity surface in Fig. 2.1, i.e., the cavity surface is perforated from φ_1 till φ_2. We have written eqs. (12) -(15) in Gaussian system of units, however, further results are dimensionless and hence valid in any system of units. To find the power P_{out} taken away from the cavity by the generated TE_{mn} mode, let us for the sake of simplicity suppose the output waveguide has the same cross section as the cavity. If mainly the desirable TE_{mn} waveguide mode with the amplitude B is generated, then P_{out} is described by the relation

$$P_{out} \;=\; |B|^2 G \tag{14}$$

and

$$G = \frac{c}{4\pi} 2\pi h_{mn} \int_0^a \left(\frac{m^2}{r^2} Z_m^2\left(\frac{\chi_{mn} r}{a}\right) + \frac{\chi_{mn}^2}{a^2}\left[Z_m'\left(\frac{\chi_{mn} r}{a}\right)\right]^2 \right) r\, dr \ , \qquad (15)$$

where h_{mn} is the waveguide propagation constant:

$$h_{mn}^2 = k^2 - \left(\frac{\chi_{mn}}{a}\right)^2 \ , \qquad (16a)$$

Z_m is the combination of Bessel and Neumann functions J_m and N_m, describing the transverse field in the cavity:

$$Z_m(\frac{\chi_{mn} r}{a}) = N_m'(\frac{\chi_{mn} a_2}{a}) J_m(\frac{\chi_{mn} r}{a}) - J_m'(\frac{\chi_{mn} a_2}{a}) N_m(\frac{\chi_{mn} r}{a}) \qquad (16b)$$

and Z_m' is its derivative; χ_{mn} is the n-th root of Z_m'. Since $P_{in} = P_{out}$, from eqs. (12) and (14) follows

$$\left|\frac{A_m}{B}\right| = \sqrt{\frac{G}{|D|}} \ . \qquad (17)$$

Let us introduce a parameter τ describing a relation between the field magnitude B in the waveguide outside the cavity and the field magnitude inside the cavity. In fact, the parameter τ describes a coupling between the cavity and the output waveguide. So, the magnetic field on the cavity inside wall ($r = a$) is:

$$\vec{H}_z^+(r = a, \varphi) = \frac{B}{\tau} \Phi_m \, e^{im\varphi} \ , \qquad (18)$$

$$\Phi_m = \frac{\chi_{mn}^2}{a^2} Z_m(\chi_{mn}) \ . \qquad (19)$$

Then the cavity quality factor Q_f is (Pereyaslavets 1985)

$$Q_f = \frac{\pi}{4\tau^2 \chi_{mn}^2} \ . \qquad (20)$$

Remembering that $P_{in} = P_{out}$, a relation between the given quality factor (eq. (19)) and the parameter ρ_1 yields from eqs. (7), (8), (17), (18) and (20).

$$\rho_1(\varphi) = \rho_{10} \, S(\varphi) \ , \qquad (21)$$

$$\rho_{10} = \frac{1}{\Phi_m}\sqrt{\frac{\pi G}{4h_m^2 Q_f |D|}} \quad . \tag{22}$$

The perforation of the cavity wall was designed in (Alexandrov et al. 1992 and 1995) with equidistant holes of the same diameter, i.e., $S(\varphi)=\sqrt{\frac{2}{\pi}}$ for $10\deg \le \varphi \le 100\deg$ and $S(\varphi) = 0$ elsewhere. However, the amplitude of the illuminating field is not uniform along the cavity wall. Using eq. (21), the distances between the holes as well as the diameters of the holes can be tapered along the wall to match the illuminating field and the field inside the cavity. This method was presented in Pereyaslavets (1995 and 1997). Such a design will increase the efficiency and decrease an undesirable counter rotating mode excitation. The illuminating field $E_\varphi^-(r=a,\varphi)$ on the cavity boundary is calculated by the computer code described above for the analysis of quasi-optical mirrors. Further the perforation tapering $S(\varphi)$ can be derived using eq. (9)

$$S(\varphi) = \frac{\left|E_\varphi^-(r=a,\varphi)\right|}{N} \quad , \tag{23}$$

where N is the factor normalizing the integral $\int_0^{2\pi}\left|S(\varphi)\right|^2 d\varphi = 1$. The N factor is given by

$$N^2 = \int_0^{2\pi}\left|\vec{E}_\varphi^-(r=a,\varphi)\right|^2 d\varphi \quad . \tag{24}$$

The perforation parameters are determined by ρ_1, therefore using eqs. (21)-(24) one could find ρ_1, i.e., the radius and the period of the perforation, by a given quality factor Q_f.

The relation between ρ_1 and the perforation parameters can be determined by the method described in Westermann and Maier (1964). The design of Alexandrov et al. (1995) is based on this method. Lets us rewrite the method of Westermann and Maier (1964) in a more convenient form.

To derive the relation between ρ_1 and the perforation parameters, let us consider an infinite, periodically perforated metallic plate.

One could define the polarizabilities of a hole (Collin 1960, p. 534). According to the Babinet's principle, the polarizabilities of the periodic system of metallic disks on a plane correspond to the polarizabilities of a dual periodic system of holes in a metallic plane, i.e., to a perforated plate. Following Collin (1960), let us use formulas for the system of

metallic disks and write down formulas for the dual pertorated plate. So, electric and magnetic dipoles for the disk are P and M (Collin 1960, p. 534 eq. (53)). The electric dipole lies on the semi-transparent plane along the incident electric field, while the magnetic dipole is in the direction normal to the surface. Let the plane wave be incident on the perforated plane with the angle γ to the normal as in Fig. 2.2. One yields:

$$\rho_1 = \frac{k}{2\beta p_\varphi p_z}(j\mathrm{P} + j\alpha\mathrm{M}) \quad , \tag{25}$$

where β is the cosine of the incident angle (i.e. $\beta = \cos(\gamma)$), α is the sine of the incident angle (i.e. $\alpha = \sin(\gamma)$), and p_φ , p_z are the system periods, i.e. the distances between the holes along φ and z directions, respectively; $k = \omega/c$, b is the holes radius and

$$\mathrm{P} = \frac{8}{3}b^3 \quad , \tag{26}$$

$$\mathrm{M} = \frac{4}{3}b^3\alpha \quad . \tag{27}$$

More accurate results are obtained if the mutual interaction field between the holes is also taken into account as part of the field acting to polarize the hole. The electric and magnetic dipole moments are thus increased by factors $(1-\alpha_e C_e)^{-1}$ and $(1-\alpha_m C_m)^{-1}$, respectively (Collin 1960, p. 535) with:

$$C_e = \frac{1.2}{\pi p_\varphi^3} - \frac{8\pi}{p_\varphi^3}\mathrm{K}_0\left(\frac{2\pi p_z}{p_\varphi}\right) \quad , \tag{28}$$

$$C_m = -\frac{1.2}{\pi p_\varphi^3} - \frac{1.2}{\pi p_z^3} + \frac{8\pi}{p_\varphi^3}\mathrm{K}_0\left(\frac{2\pi p_z}{p_\varphi}\right) + \frac{8\pi}{p_z^3}\mathrm{K}_0\left(\frac{2\pi p_\varphi}{p_z}\right) \quad , \tag{29}$$

where K_0 is the modified Bessel function; $\alpha_e = -\frac{16}{3}b^3$ and $\alpha_m = -\frac{8}{3}b^3$. The formulas above are valid when the perforation period is less than one third of the wavelength. When the periods p_φ and p_z increase, the electric and magnetic dipole moments are to be further increased by an empirical factor of 1.4. To take the wall thickness into account, each hole is considered as a circular 'below cutoff' waveguide with the dominant mode $TE_{1,1}$.

Equations (25)-(29) were compared with the experimental results by Keilmann (1980) and Roberts et al. (1994) as well as with the measurements performed at the Forschungszentrum Karlsruhe, Germany. A perforated plate was manufactured with the wall thickness of 0.5mm, the period of perforation of 1 mm and the diameter of the holes 0.75 mm. Its transmission was measured at several frequencies near 140 GHz. Equations (25) - (29) give a transmission of the plate of -21.5 dB. The measured transmission is equal to 23dB ± 3dB, i.e., in a good agreement with the theory.

Employing the method described above, the low power mode generators were designed for $TE_{15,3}$ mode at 84 GHz and for $TE_{31,8}$ mode at 168 GHz.

The design of the coaxial cavity for the $TE_{15,3}$ mode generator at 84 GHz is shown in Fig. 2.3 and the design of the perforated wall of the straight cavity section, whose external radius R is 14.96 mm, is presented in the Table 2.1 for the perforated wall thickness of $d = 0.4$ mm. The coordinate center for the data in the Table 2.1 corresponds to the cavity center in Fig. 2.1. The period along $0z$ axis (perpendicular to the figure plane) is p_z . The period p_z must be changed from row to row. To decrease the manufacturing process, the number of different hole diameters is minimized as shown in the Table 2.1. Six different drills only are employed. The field distribution along the cavity of the $TE_{15,3}$ mode generator is shown in Fig. 2.4.

The mirror design for the $TE_{15,3}$ mode generator is presented in Fig. 2.5. The parameters of the Gaussian beam illuminating this mirror are following: its waist radius corresponding to the 1/e width of the field amplitude is 25.1 mm, the waist center location is x=15 mm and y = 45 mm. The mirror is designed to illuminate the cavity surface from φ=95.2 to 193.3 degrees.

Preliminary results for the $TE_{15,3}$ mode generator indicate the resonant frequency at 84.09GHz - very good agreement with the designed frequency. To increase the mode purity, a microwave absorber was placed in the cavity cut-off section, i.e. at $0 < z < 6$ mm in Fig. 2.3. The thickness of the absorbing layer is evaluated from the field distribution in the cavity shown in Fig. 2.4. The near field structure at the output aperture is shown in Fig. 2.6 for the vertical polarization. Analysis of the output mode purity should be accomplished later. As it was explained in Alexandrov (1995), a small percentage of contra-rotating mode essentially affects the near field pattern and is the cause of knots in the Fig. 2.6. However, the estimated amount of the contra-rotating mode in the Fig. 2.6 is about 7% only.

The design of the coaxial cavity for the $TE_{31,8}$ mode generator at 168 GHz is shown in Fig. 2.7 and the field of the $TE_{31,8}$ mode in this cavity in Fig. 2.8. The design of the perforated wall of the straight cavity section, whose external radius R is 17.99 mm, is presented in the Table 2.2 for the perforated wall thickness of d=0.4mm. Again, according to Fig. 2.1, the period p_z along $0z$ axis must be changed from row to row. Three different drills only are employed.

As it follows from the field distribution along this cavity shown in Fig. 2.8, the holes in this design are punched not only along the straight cavity section, i.e. from $z = 30$ mm till $z = 74$ mm, but also along the uptaper from $R = 17.99$ mm to $R = 18.11$ mm, i.e. from

$z = 74$ mm till $z = 85$ mm, so the total uptaper length is 55mm. This uptaper section is relatively long, it was designed to match the low power mode-generator output with the previously designed Toshiba uptaper and this section must be perforated, since the field amplitude there is relatively large (see Fig. 2.8). The perforation decreases the cut off frequency, since it increases effective radius.

The mirror design for the $TE_{31,8}$ mode generator at 168 GHz is presented in the Fig. 2.9. The parameters of the Gaussian beam illuminating this mirror are following: its waist radius corresponding to 1/e width of the field amplitude is 25.0 mm, the waist center is located at $x = 8$ mm and $y = 43$ mm. The waist radius of the illuminating Gaussian beam was chosen comparing simulation results for different radii, including 20.0 mm, 25.0 mm and 30.0 mm. The mirror is designed to illuminate the cavity surface from $\varphi = 118.5$ to 208.8 degrees.

3. Analysis of RF power in a cold gyrotron cavity

For the CW operation of a high-power gyrotron, RF power penetration in the beam tunnel (Fig. 3.1) may be a serious problem. One could estimate such power leakage analyzing the cold gyrotron cavity without electron beam. The cavity in Fig. 3.1 is composed of the beam tunnel, the cut-off section preventing RF power leakage in the beam tunnel, the straight cavity section for the interaction of the electron beam with the RF field of the desired resonant mode and the output uptaper to guide the output RF power to a mode converter and/or a quasi-optical unit. Here we analyze a design of the cut-off cross section to prevent RF power penetration in the beam tunnel and consequent decrease of the output gyrotron power.

First, one should determine the resonant frequency of the desired mode in the cavity. Following Edgecombe (1993), the resonant frequency and the quality factor of the cavity are obtained by numerical solution of the Vlasov equation. A computer code employed in a standard design procedure of a gyrotron cavity can be applied to this problem. One of the computed field profiles for $TE_{31,8}$ mode in the cavity from Fig. 3.1 is shown in Fig. 3.2.

One does not need to take into account a mode conversion to obtain the resonant frequency, so a computer code solving a single-mode Vlasov equation can be employed. However, one has to take the mode conversion into account to compute the RF power leakage into the beam tunnel. One could implement the procedure described later in this section, if a computer code solving Vlasov type equation for multiple modes is not available.

At the resonant frequency one can consider an incidence of the desired mode on a cross section of the gyrotron cavity. To analyze the mode conversion, we have applied a computer code based on the scattering matrix approach. It is similar to the one mentioned in Edgecombe (1993). We analyzed the RF power leakage into the beam tunnel, the left hand side of the cross section J1-J2 in Fig. 3.1, for several cavity designs.
The operating $TE_{22,6}$ or $TE_{31,8}$ mode is incident either from the right hand side of the cross section S1-S2 or from the right hand side of the cross section U1-U2. The computed RF

power leakage in the beam tunnel is more close to the real gyrotron operation if the operating mode is incident on the cross section U1-U2. We have compared those results with the ones for the operating mode incident on the cross section S1-S2. This conclusion is valid only if the output uptaper section is properly designed, i.e., the mode conversion in the output uptaper is relatively small. So at the resonant frequency of the cavity, if the operating mode is incident from the right hand side of the cross section U1-U2, a resonant field is excited in the cavity. The structure of the resonant field is essentially independent on the excitation. Hence, at the resonant frequency, the RF field at the cross section S1-S2 has approximately the same value for two problems: an electron beam exciting the cavity in a real gyrotron operation or the operating mode incident from the right hand side of the cross section U1-U2. One can also estimate a low limit of the RF power leakage analyzing the incidence of the operating mode from the right hand side of the cross section S1-S2.

This method was applied to analysis of some Toshiba gyrotron cavity designs. An example of computation for an early design of $TE_{31,8}$ cavity at 168.13 GHz ($\alpha = 0$) is given in the Table 3.1 and 3.2. According to a numerical calculation, the total mode conversion of this design in the output uptaper from the U1-U2 cross section till the beginning of the straight cavity section is equal to 0.07%, in the case when the $TE_{31,8}$ mode is incident from the U1-U2 cross section. Therefore, the method described above can be employed for the numerical analysis of this design. The reflection coefficients at the U1-U2 cross section are shown in the Table 3.1. Obviously, the main part of the incident power is reflected. The transmission coefficients corresponding to the power leakage in the beam tunnel are presented in the Table 3.2. If the $TE_{31,8}$ mode is incident from the right hand side of the S1-S2 cross section, the computed total transmission to the beam tunnel (i.e. power leakage) is equal to 0.22%. A relatively high power leakage of this design is caused by the mode conversion in the cut-off cross section between S1-S2 and K1-K2 cross section. As it follows from the Table 3.2, the $TE_{31,7}$ and $TE_{31,8}$ modes are in cut-off in this section. However, they are partly coupled to the $TE_{31,6}$ mode penetrating to the beam tunnel. To diminish such a leakage, one has to decrease the angle of the linear taper between the cross-sections S1-S2 and K1-K2 and hence increase its length. The increase of the total length could be probably compensated through a modification of the nonlinear output uptaper.

4. Analysis of non-linear waveguide uptapers.

The computer code employing scattering matrix approach was mentioned in the previous section. This code was applied to the analysis of the mode conversion losses in some nonlinear uptapers at 84 GHz and 168 GHz.

As an example, let us consider a Varian output uptaper at 84 GHz with the input diameter 31.446 mm and with the output diameter 50.8 mm for the $TE_{15,3}$ mode. This is an old design developed several years ago and is considered here mainly for illustration purposes. Recent Varian uptapers have other parameters. The results for this uptaper are given in the Table 4.1.

Usually the output uptapers are designed by minimizing the coupling of the desired mode to the main parasitic mode. One assumes the coupling to other parasitic modes being of the same order of magnitude. Such an assumption is a good approximation for short pulse gyrotron operations. However, for CW high power operation a more detailed analysis is required.

The uptaper was obviously designed to minimize the conversion losses to the $TE_{15,2}$ forward (transmitted) wave - as it follows from Table 4.1 the coupling to this wave is 0.18% only. At the same time, the coupling to the transmitted $TE_{15,4}$ wave is relatively large: 1.25% - those conversion losses can pose a problem for some CW applications. For example, the uptaper conversion losses of 1.5% correspond to 7.5 kW power losses at 0.5 MW level of output CW power and combined with the losses of quasi-optical unit may pose a tube heating problem. For those applications more sophisticated uptapers should be developed. The uptaper design could be an iterative process. First an uptaper is designed for some conversion losses to the selected parasitic mode, then total power losses are analyzed and another coupling coefficient to a parasitic mode is selected. The iterative process continues until total conversion losses will be minimized for the given length. On the other hand, for the uptaper considered in the Table 4.1 the coupling to the reflected waves is very small (less than 0.004%). The coupling coefficients to the transmitted TM waves are small as well, the maximal coupling coefficient being 0.01% only. So, further optimization for reflected waves and for TM modes is not required.

5. Conclusion

1. Low power generators of the rotating gyrotron type modes (the $TE_{15,3}$ mode at 84 GHz and the $TE_{31,8}$ mode at 168 GHz) have been developed and analyzed. Preliminary testing of $TE_{15,3}$ mode generator at 84 GHz is accomplished.
2. RF power leakage was analyzed for high power Toshiba gyrotron cavities at 168 GHz. Some practical recommendations were elaborated.
3. Nonlinear uptapers for high power gyrotrons were analyzed, including Varian uptaper at 84 GHz and some 168 GHz uptapers. It is demonstrated that a more detailed conversion losses analysis is required for high power CW operation.

6. Acknowledgment

The authors would like to thank Drs. T. Watari, M. Fujiwara and A. Iiyoshi for their continuing encouragement. They also acknowledge the mechanical design performed by Mr. S. Ito. One of the authors, Dr. M. Pereyaslavets, was supported by a JSPS fellowship.

References

Alexandrov, N.L., Chirkov, A.V., Denisov, G.G., Vinogradov, D.V, Kasparek, W., Pretterebner, J., and Wagner, D., 1992, Selective excitation of high-order modes in circular waveguides. International Journal of Infrared and Millimeter Waves, v. 13, no. 9, p. 1369-1385.

Alexandrov, N.L., Denisov, G.G., Whaley, D.R., and Tran, M.Q., 1995, Low power excitation of gyrotron-type modes in a cylindrical waveguide using quasi-optical techniques. International Journal of Electronics, 79, no. 2, p. 215-226.

Braz O., Kern S., Losert M., Möbius A., Pereyaslavets M. and Thumm M., 1995, Improvements of Mode Converters for Low Power Excitation of Gyrotron-Type Modes - In: The 20th International Conference on Infrared and Millimeter Waves. Lake Buena Vista (Orlando), Florida - Conference Digest, p. 471-472.

Braz O., Arnold A., Losert M., Möbius A., Pereyaslavets M., Thumm M. and Malygin V.I., 1996, Low Power Excitation and Mode Purity Measurements on Gyrotron-Type Modes of High Order - In: The 21st International Conference on Infrared and Millimeter Waves Humboldt University at Berlin, Germany - Conference Digest.

Collin, R.E., 1960, Field Theory of guided waves (NY, USA: McGraw-Hill).

Denisov, G.G., Kuftin, A.N., Malygin, V.I., Venediktov, N.P., Vinogradov, D.V., and Zapevalov, V.E., 1992, 110 GHz gyrotron with a built-in high-efficiency converter. International Journal of Electronics, v. 72, nos. 5--6, p. 1079-1091.

(Edgecombe C.J. - editor), 1993, Gyrotron oscillators: their principles and practice. (Washington DC: Taylor and Francis), 423 p.

Keilmann, F., 1980, Infrared high-pass filter with high contrast. International Journal of Infrared and Millimeter Waves, v. 2 , no. 2, p. 259-272.

Pereyaslavets M., 1985, Synthesis of waveguide filter and mode converter with a decreased non-resonant pedestal. Soviet Journal of Communication Technology and Electronics, v. 30 , no. 3, p. 133--138.

Pereyaslavets M., Braz O., Kern S., Losert M., Möbius A. and Thumm M., 1997, Improvements of Mode Converters for Low Power Excitation of Gyrotron-Type Modes. International Journal of Electronics. v.82, no.1.

Pereyaslavets M., Braz O., Kern S., Losert M., Möbius A. and Thumm M., 1996, Low Power Excitation of Gyrotron-Type Modes. Mode Exciters - In: The 13th Annual

Conference of the Japan Society of Plasma Science and Nuclear Fusion Research, Kyoto University. - Conference Reports, Report 21pA3, p. 124.

Roberts, A., von Bibra, M.L., Gemünd, H.-P., and Kreysa, E., 1994, Thick grids with circular apertures: a comparison of theoretical and experimental performance. International Journal of Infrared and Millimeter Waves, v. 15 , no. 3, p. 505--517.

Silver, S., 1984, Chapter 5.7: Current distribution method. Microwave Antenna Theory and Design. Editors: Silver, S., and James, H.M. (London, UK: Peter Peregrinus).

Vlasov, S.N., and Shapiro, M.A., 1989, Use of bi-involute mirrors to transport caustic surfaces. Soviet Technical Physics Letters , v. 15 , no. 5, p. 374-375.

Wada O., Hashimoto M. and Nakajima M., 1988, Calculation of radiation from a quasi-optical reflector antenna for whispering gallery mode. International Journal of Electronics, v. 65, no. 3, p. 725-732.

Westermann, F., and Maier, W., 1964, Das Fabry-Perot-Interferometer im Mikrowellengebiet. Zeitschrift für Physik, v. 179, no. 1, p. 244--255.

Captions to Illustrations

Figure 2.1: Schematic of low power mode generator

Figure 2.2: Analysis of field penetration through the perforated plate

Figure 2.3: Coaxial cavity for the $TE_{15,3}$ mode generator at 84 GHz

Figure 2.4: Field in the cavity of the low power $TE_{15,3}$ mode generator at 84 GHz

Figure 2.5: Mirror design for the $TE_{15,3}$ mode generator

Figure 2.6: Measured field pattern for the $TE_{15,3}$ mode generator at 84.09 GHz

Figure 2.7: Cavity design for the low power $TE_{31,8}$ mode generator at 168 GHz.

Figure 2.8: Field in the cavity of the low power $TE_{31,8}$ mode generator at 168 GHz.

Figure 2.9: Mirror design for the $TE_{31,8}$ mode generator

Figure 3.1: Schematic of high power gyrotron cavity

Figure 3.2: Field in the gyrotron cavity computed in the single mode approximation

Table 2.1. Design of the perforated cavity wall for the $TE_{15,3}$ mode generator at 84 GHz

Six hole diameters are employed: 1.5mm; 1.4mm; 1.3mm; 1.2mm; 1.0mm and 0.8mm.

φ degrees	p_z mm	hole diameter mm	number of holes
93.1	1.7	0.8	19
98.6	1.6	0.8	20
104.8	1.7	1.0	19
109.8	1.2	1.0	28
114.7	1.6	1.2	20
120.5	1.5	1.2	22
126.0	1.4	1.2	24
131.8	1.5	1.3	22
138.0	1.6	1.4	21
144.6	1.7	1.5	20
151.2	1.7	1.5	20
157.8	1.7	1.5	20
164.4	1.6	1.4	24
170.6	1.4	1.2	21
176.5	1.2	1.0	28
181.3	1.2	1.0	28
186.6	1.3	1.0	25
192.1	1.1	0.8	30
196.7	1.7	0.8	19
203.3	1.7	0.8	19

Table 2.2. Design of the perforated cavity wall for the $TE_{31,8}$ mode generator at 168 GHz

Three hole diameters are employed: 0.65 mm; 0.55 mm and 0.5 mm

φ degrees	p_z mm	hole diameter mm	number of holes
103.2	0.80	0.5	69
105.7	0.80	0.5	69
108.0	0.70	0.5	79
120.4	0.75	0.55	73
123.1	0.85	0.65	65
125.7	0.85	0.65	65
128.4	0.85	0.65	65
131.1	0.85	0.65	65
133.7	0.85	0.65	65
136.4	0.85	0.65	65
139.1	0.85	0.65	65
141.8	0.85	0.65	65
144.5	0.85	0.65	65
147.1	0.85	0.65	65
149.8	0.85	0.65	65
152.5	0.85	0.65	65
155.2	0.85	0.65	65
157.9	0.85	0.65	65
160.6	0.85	0.65	65
163.3	0.85	0.65	65
165.9	0.85	0.65	65
168.6	0.85	0.65	65
171.3	0.85	0.65	65
174.0	0.85	0.65	65
176.7	0.85	0.65	65
179.4	0.85	0.65	65
182.1	0.85	0.65	65
184.8	0.85	0.65	65
187.4	0.85	0.65	65
190.1	0.85	0.65	65
192.8	0.85	0.65	65
195.5	0.85	0.65	65
198.1	0.75	0.55	73
200.4	0.85	0.50	65

Table 3.1. $TE_{31,8}$ **mode incident on a gyrotron cavity at 168 GHz. Power Reflection coefficients in %**

$TE_{31,1}$	5.59802E-03
$TE_{31,2}$	1.95734E-02
$TE_{31,3}$	3.65709E-02
$TE_{31,4}$	4.59691E-02
$TE_{31,5}$	3.91917E-02
$TE_{31,6}$	0.643405
$TE_{31,7}$	0.339636
$TE_{31,8}$	97.3626
$TE_{31,9}$	5.53617E-02
$TE_{31,10}$	2.45926E-02
----------	----------
$TM_{31,1}$	1.56830E-03
$TM_{31,2}$	2.23033E-03
$TM_{31,3}$	4.46945E-03
$TM_{31,4}$	1.20513E-03
$TM_{31,5}$	3.58983E-03
$TM_{31,6}$	5.03966E-02
$TM_{31,7}$	0.866814
$TM_{31,8}$	3.25785E-03
$TM_{31,9}$	3.89068E-04
$TM_{31,10}$	5.48398E-04

Table 3.2. $TE_{31,8}$ **mode incident on a gyrotron cavity at 168 GHz.**

Power TRANSMISSION coefficients (i.e. power leakage into the beam tunnel) in %

$TE_{31,1}$	2.05743E-03
$TE_{31,2}$	4.13516E-03
$TE_{31,3}$	7.02469E-02
$TE_{31,4}$	1.76694E-02
$TE_{31,5}$	6.40561E-02
$TE_{31,6}$	**0.223493**
$TE_{31,7}$	1.19757E-02
$TE_{31,8}$	4.41883E-04
$TE_{31,9}$	1.04613E-04
Total transmission of TE **modes**	**0.4%**
---	---
$TM_{31,1}$	2.50127E-03
$TM_{31,2}$	5.32069E-03
$TM_{31,3}$	6.66125E-03
$TM_{31,4}$	3.27439E-03
$TM_{31,5}$	1.83386E-02
$TM_{31,6}$	6.09426E-02
$TM_{31,7}$	1.58257E-03
$TM_{31,8}$	1.51083E-04
$TM_{31,9}$	2.81858E-05
Total transmission of TM **modes**	**0.1%**
Total transmission of TE **and** TM **modes**	**0.5%**

Table 4.1. Varian uptaper at 84 GHz (input diam=31.446 mm; output diam=50.8mm)

Power Reflection coefficients in %		
TE 15, 1	2.78800E-04	
TE 15, 2	1.68022E-04	
TE 15, 3	2.56677E-03	
---	---	---
TM 15, 1	2.21200E-03	
TM 15, 2	1.19026E-03	
Power TRANSMISSION coefficients in %		
TE 15, 1	6.27438E-02	
TE 15, 2	0.179007	-27.5 dB
TE 15, 3	98.0399	main mode
TE 15, 4	**1.24731**	-19.1 dB maximal parasitic
TE 15, 5	8.64323E-02	
TE 15, 6	0.136027	-28.7 dB
TE 15, 7	6.12451E-03	
TE 15, 8	3.44673E-03	
---	---	---
TM 15, 1	3.05458E-02	
TM 15, 2	3.92444E-02	
TM 15, 3	9.53879E-02	-30dB
TM 15, 4	1.19418E-02	
TM 15, 5	2.87091E-02	
TM 15, 6	2.45584E-02	
TM 15, 7	2.23730E-03	

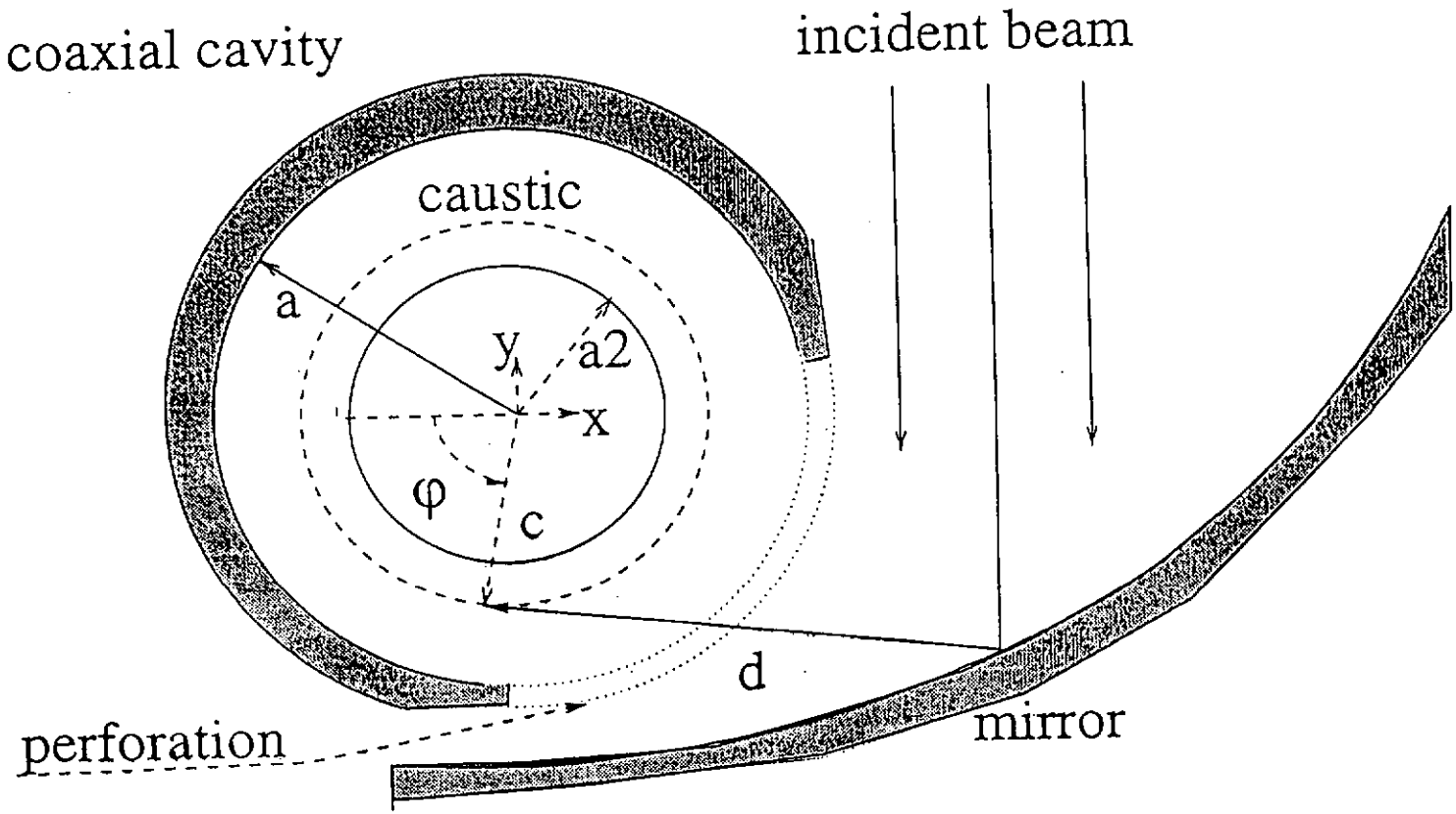

Fig. 2.1 Schematic of mode generator

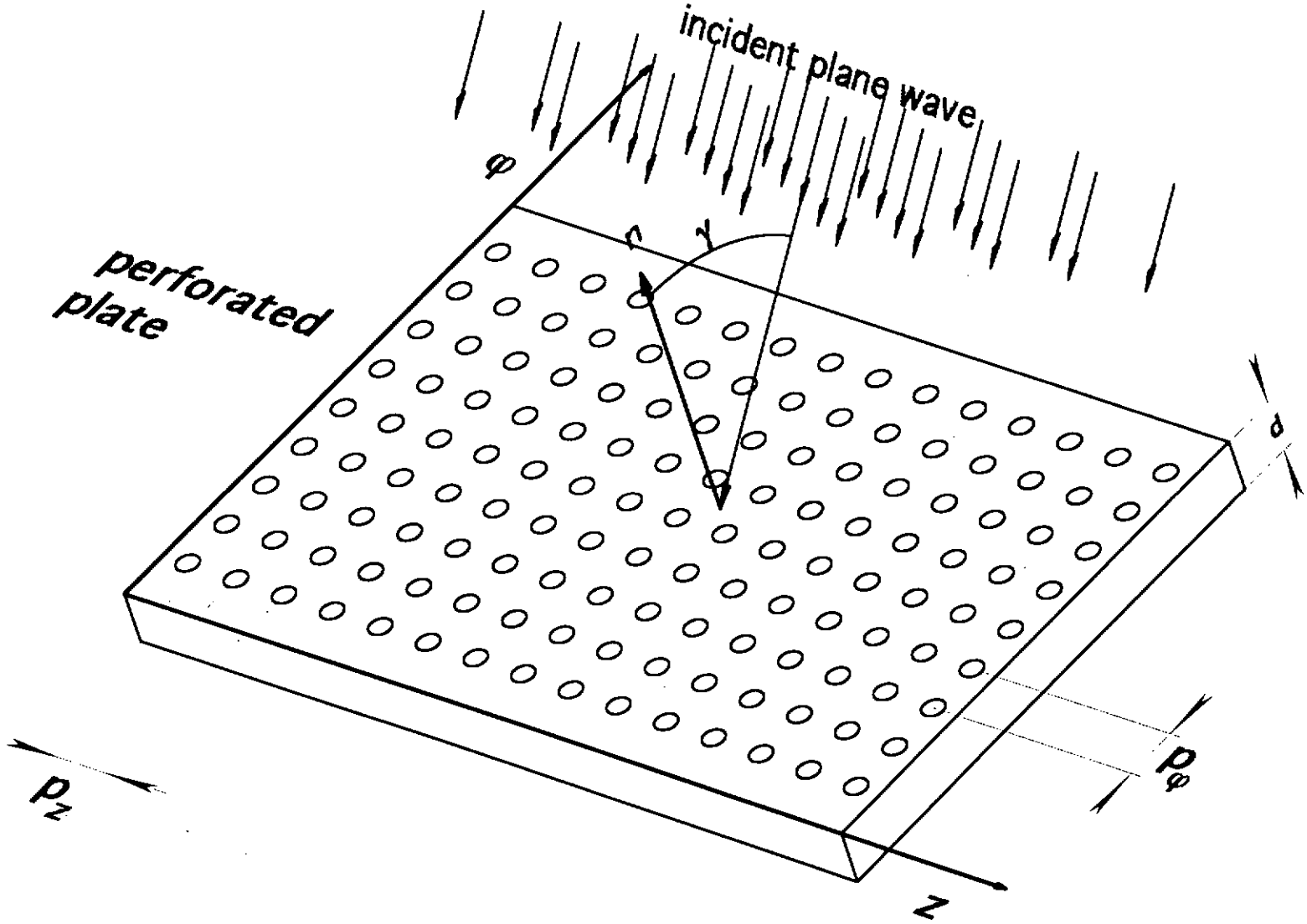

Fig. 2.2 Analysis of field penetration through the perforated plate

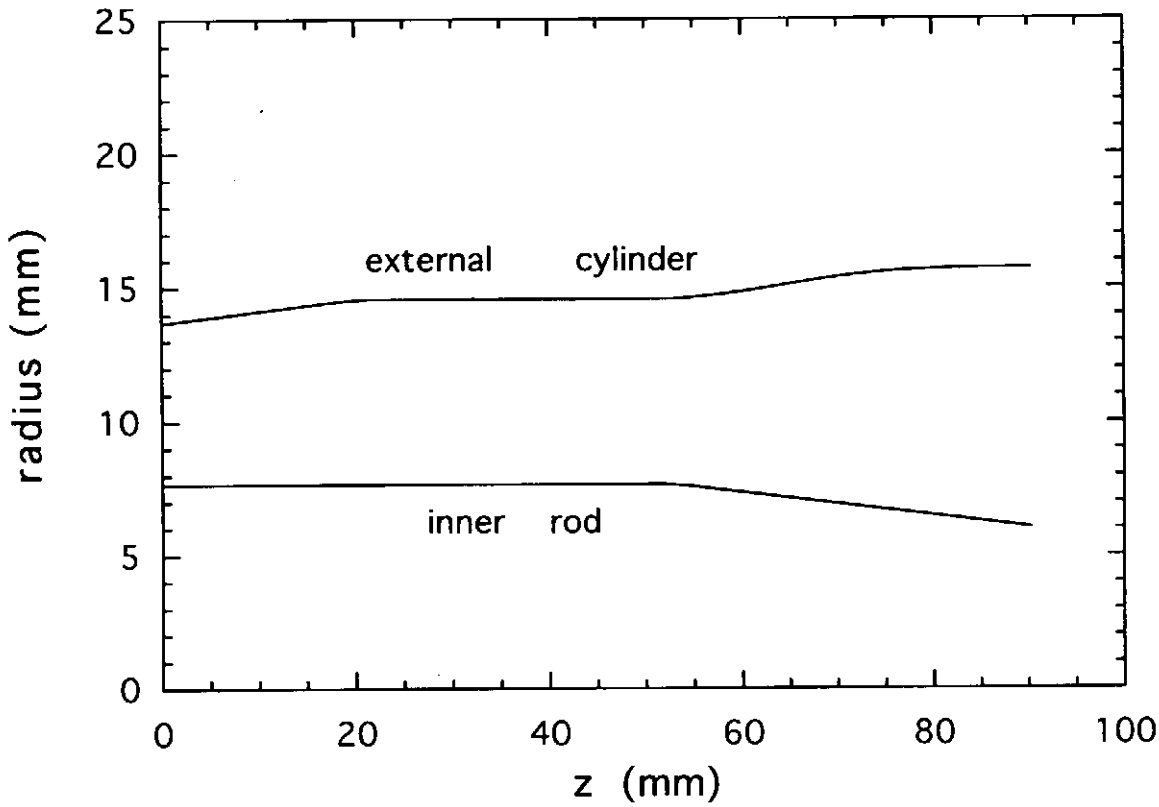

Fig. 2.3 Coaxial cavity for $TE_{15,3}$ mode generator at 84 GHz

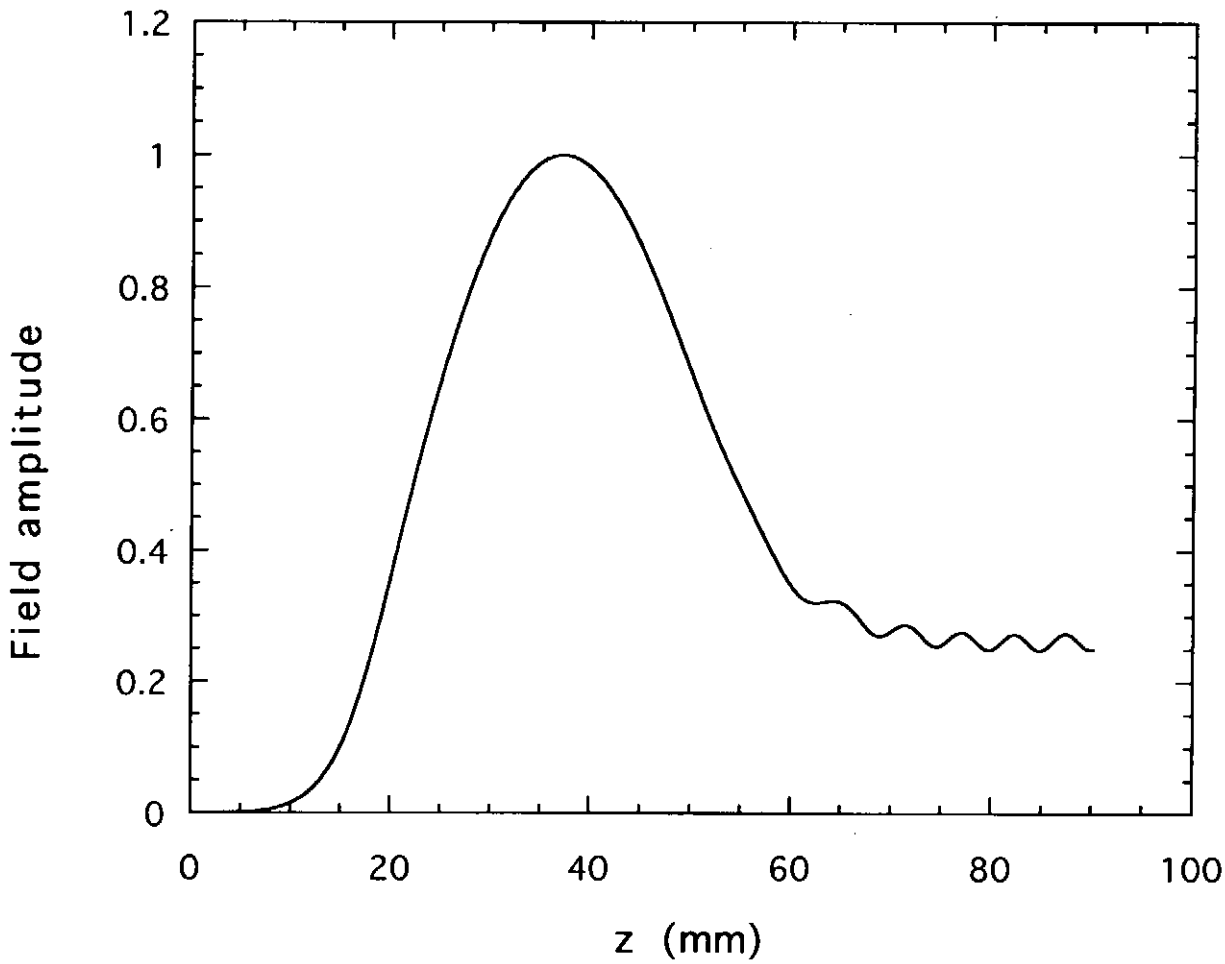

Fig. 2.4 Field in the cavity of the low power $TE_{15,3}$ mode generator at 84 GHz

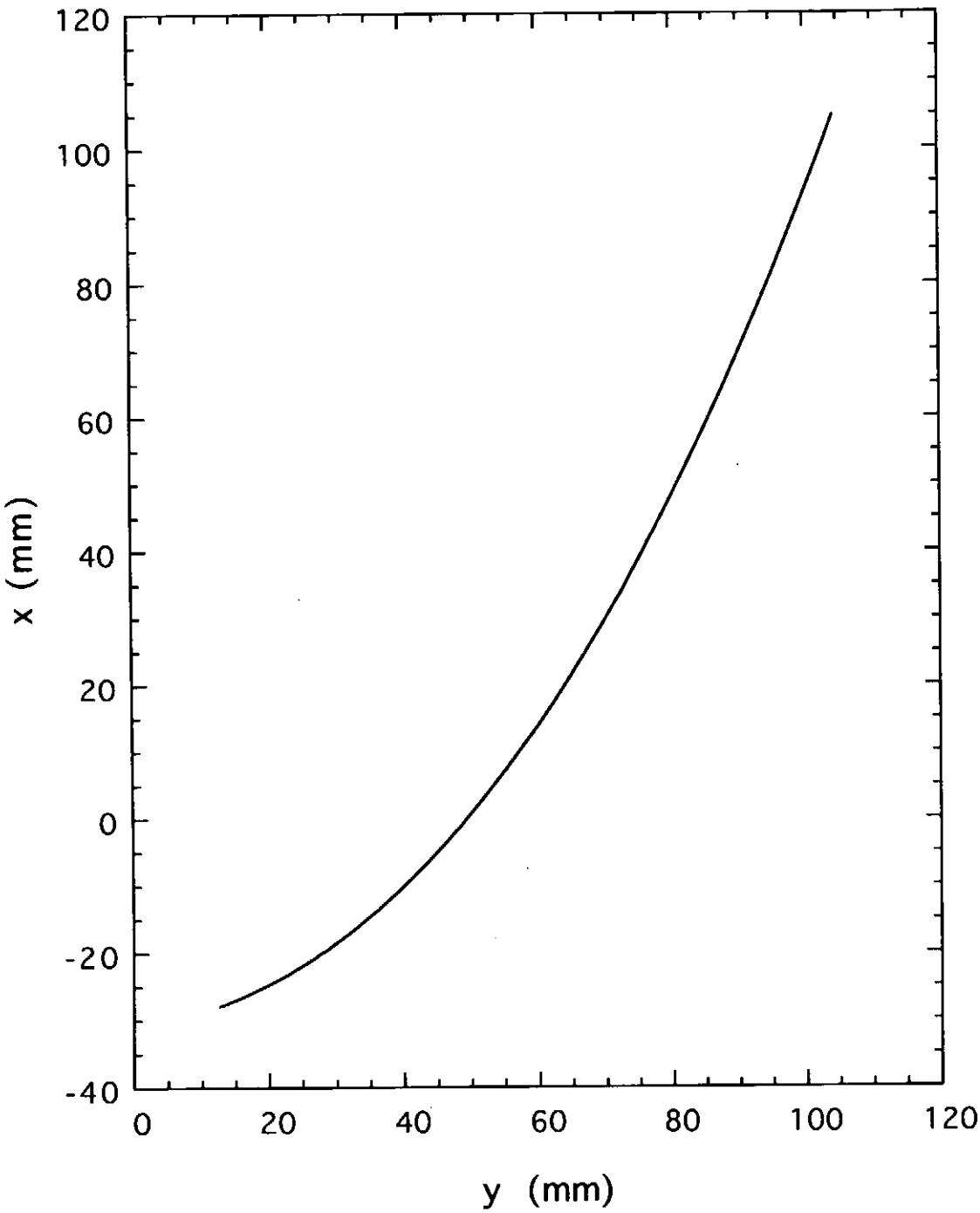

Fig. 2.5 Mirror design for $TE_{15,3}$ mode generator

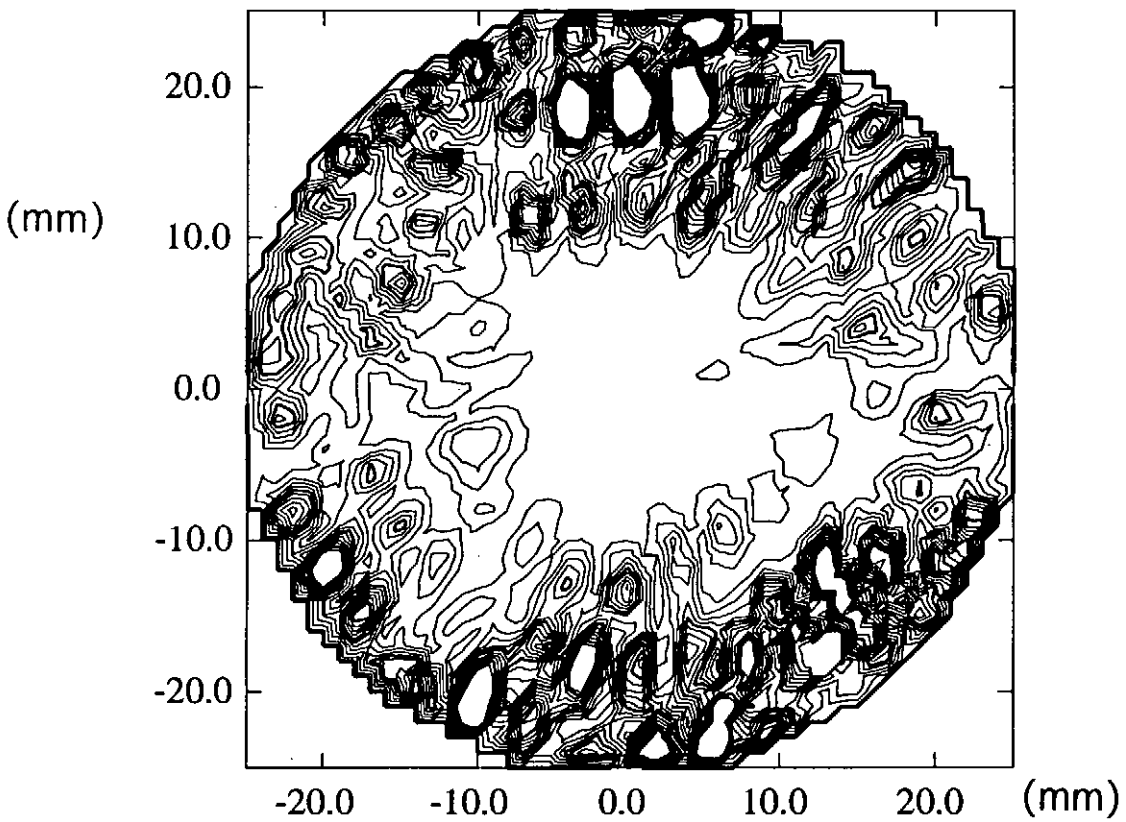

Fig. 2.6 **Measured field pattern for the $TE_{15,3}$ mode generator at 84.09 GHz**

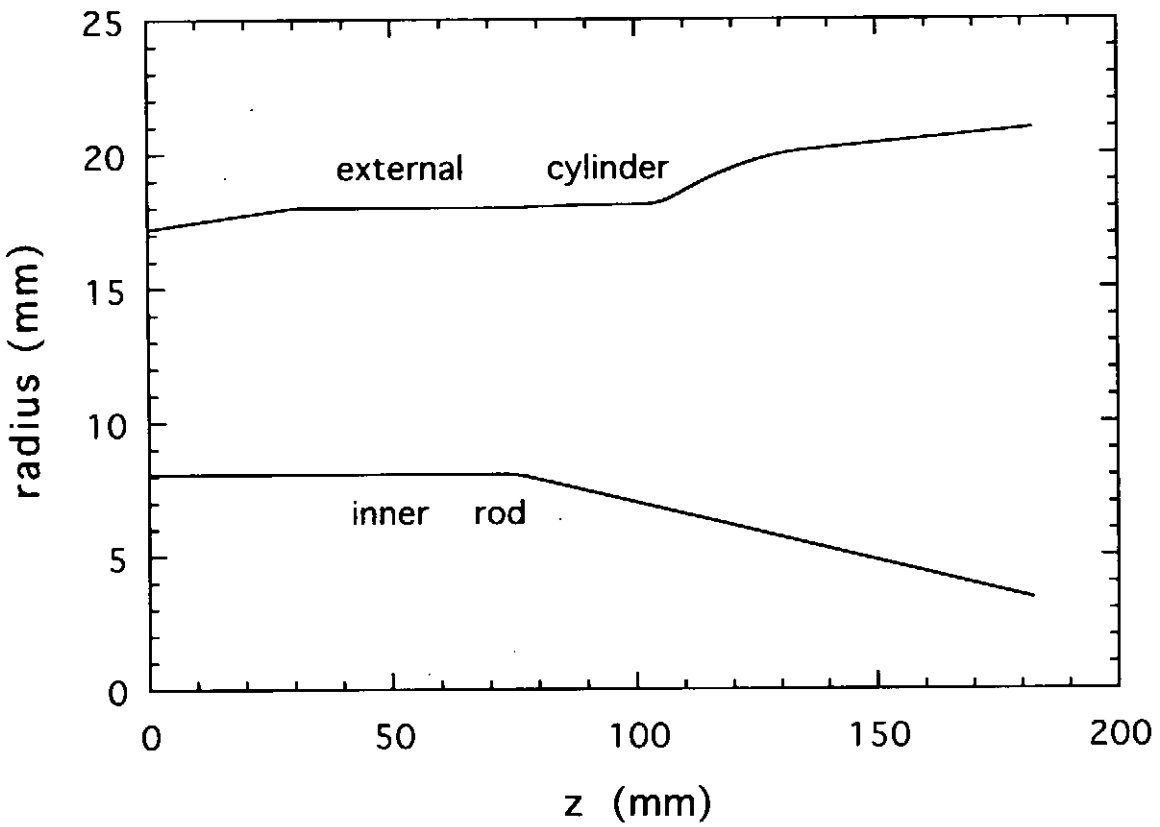

Fig. 2.7 Cavity design for the low power $TE_{31,8}$ mode generator at 168 GHz

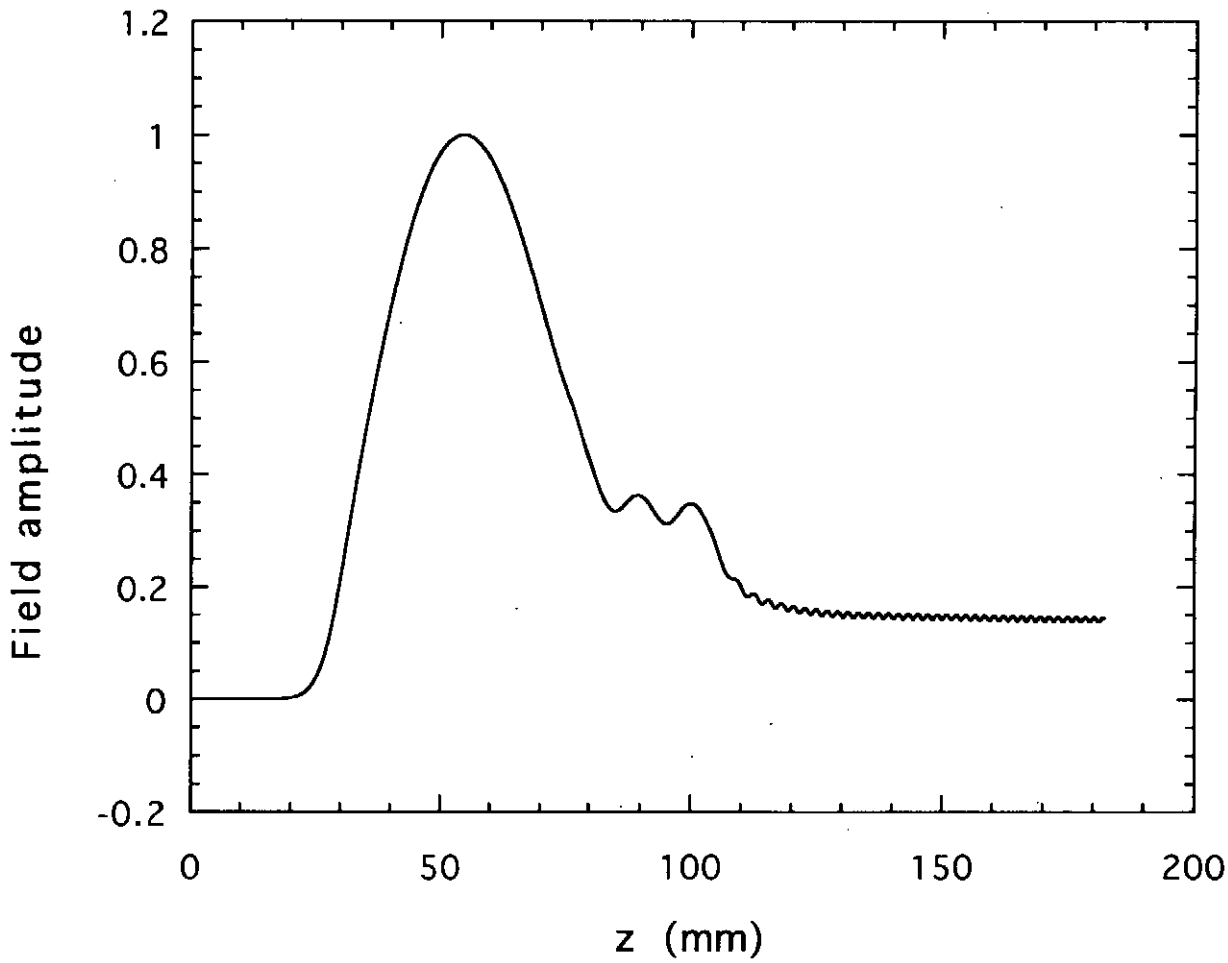

Fig. 2.8 Field in the cavity of the low power $TE_{31,8}$ mode generator at 168 GHz

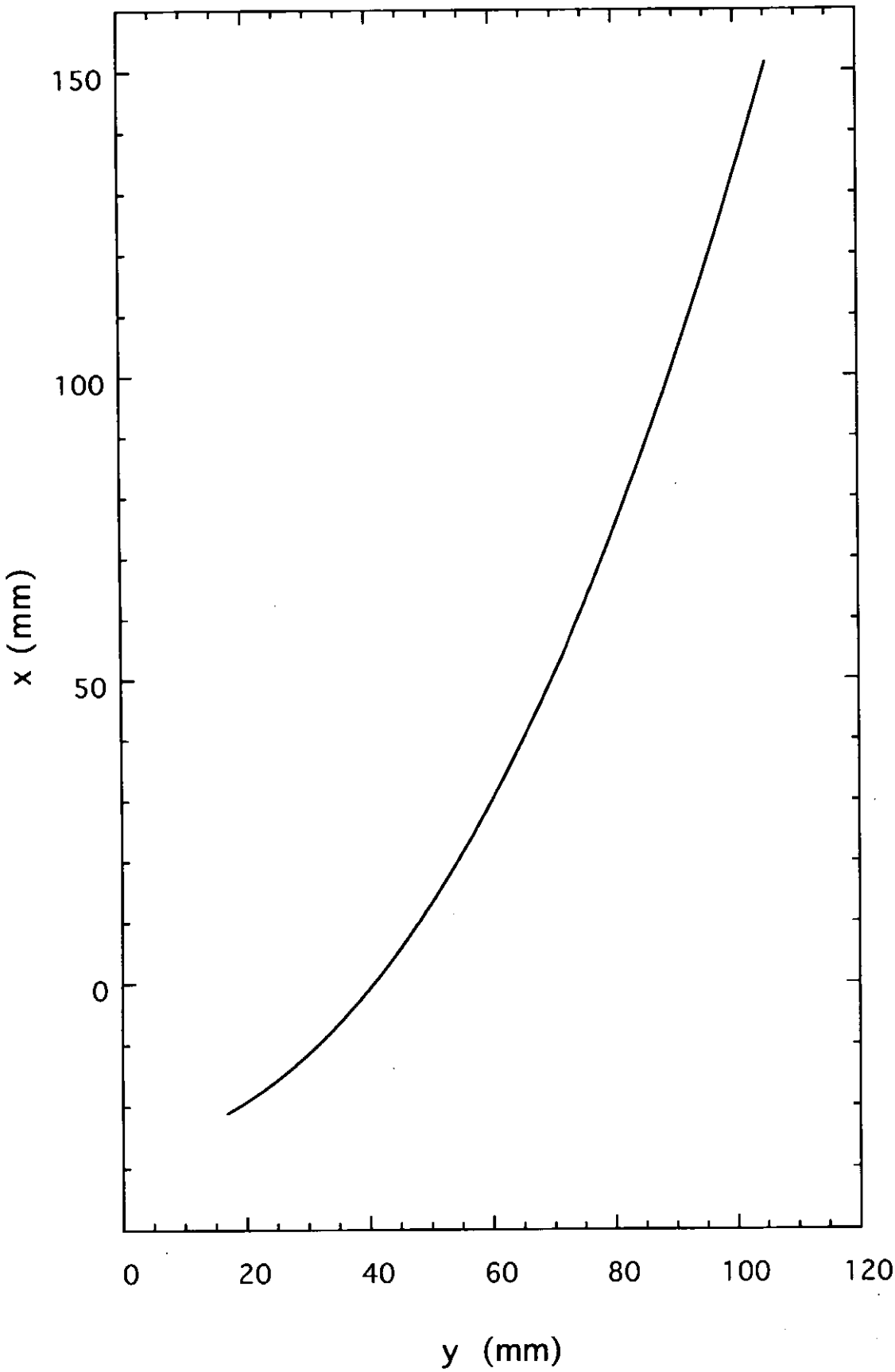

Fig. 2.9 Mirror design for $TE_{31,8}$ mode generator

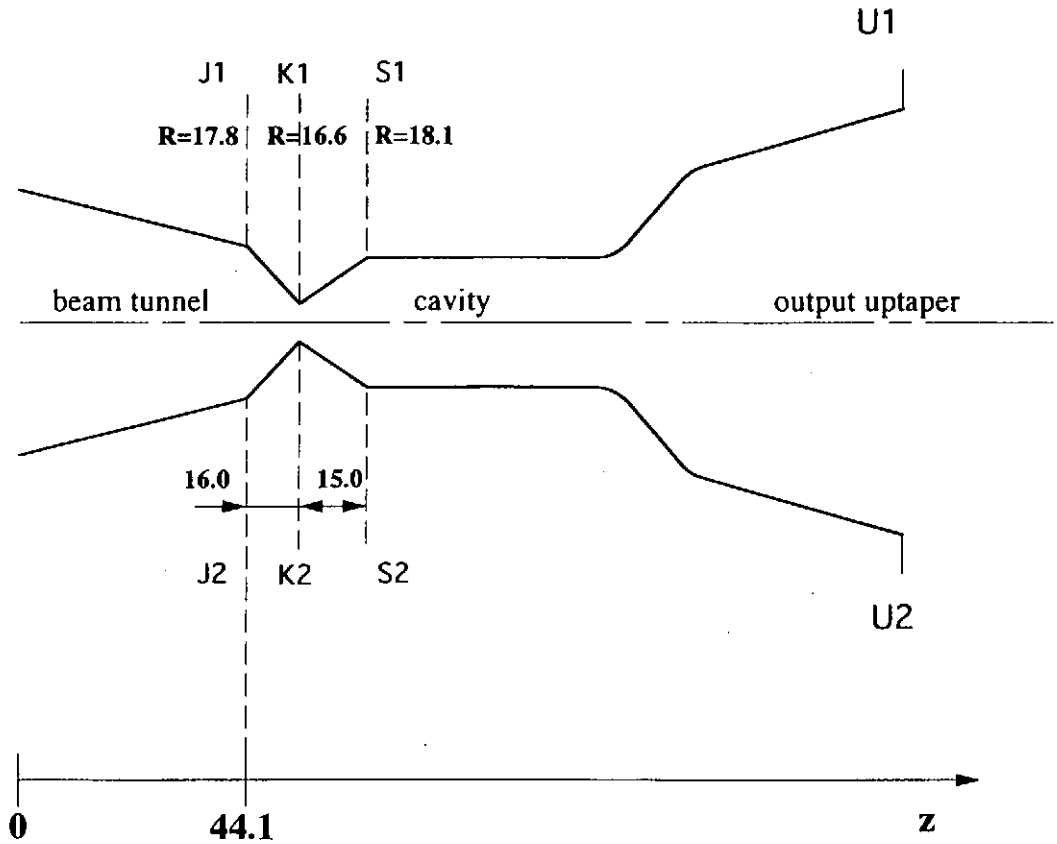

Fig. 3.1 High power gyrotron cavity, $TE_{31,8}$ mode, 168 GHz

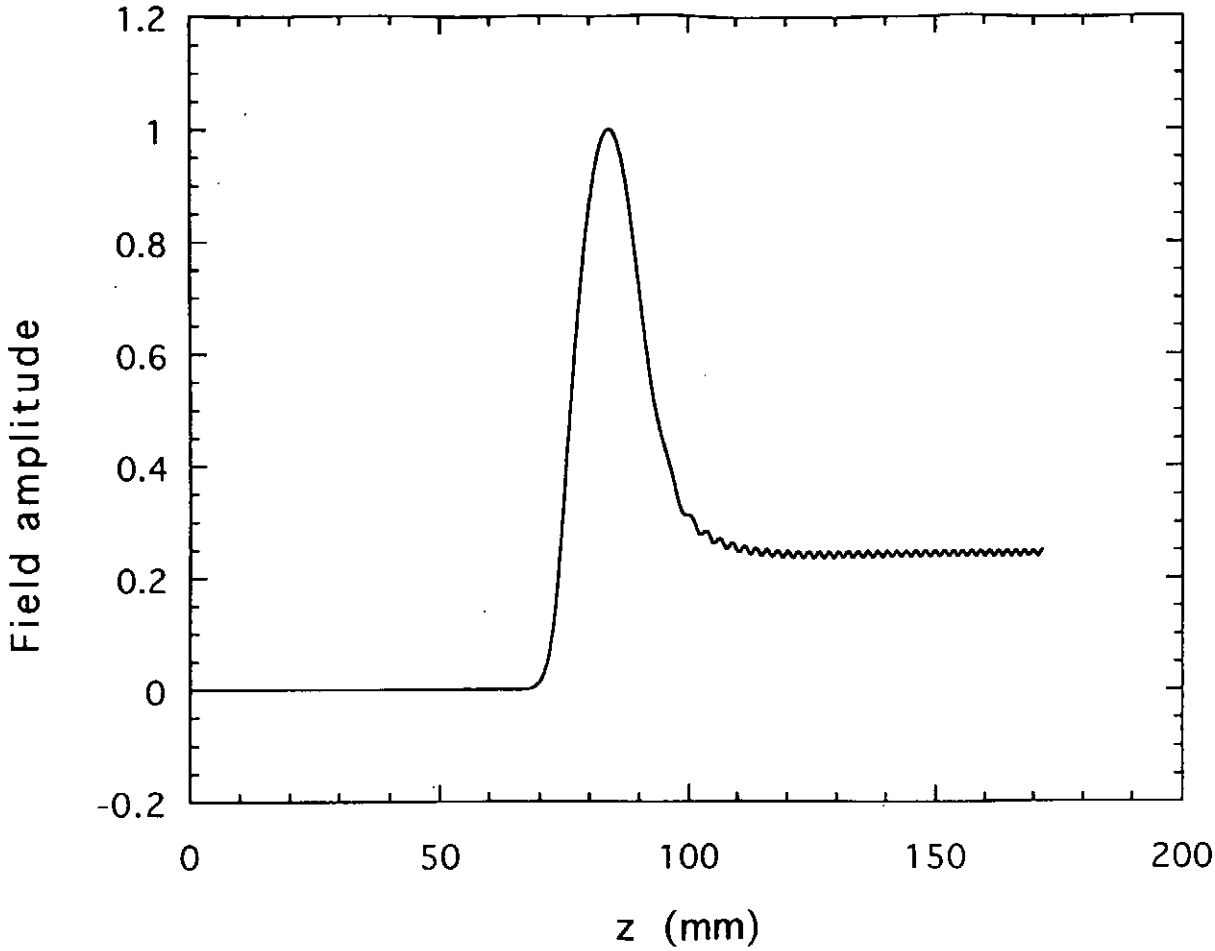

Fig. 3.2 Field in the high power gyrotron cavity, single mode approximation at 168 GHz, $TE_{31,8}$ mode

Recent Issues of NIFS Series

NIFS-426 H. Kitauchi, K. Araki and S. Kida,
Flow Structure of Thermal Convection in a Rotating Spherical Shell; July 1996

NIFS-427 S. Kida and S. Goto,
Lagrangian Direct-interaction Approximation for Homogeneous Isotropic Turbulence; July 1996

NIFS-428 V.Yu. Sergeev, K.V. Khlopenkov, B.V. Kuteev, S. Sudo, K. Kondo, F. Sano, H. Zushi, H. Okada, S. Besshou, T. Mizuuchi, K. Nagasaki, Y. Kurimoto and T. Obiki,
Recent Experiments on Li Pellet Injection into Heliotron E; Aug. 1996

NIFS-429 N. Noda, V. Philipps and R. Neu,
A Review of Recent Experiments on W and High Z Materials as Plasma-Facing Components in Magnetic Fusion Devices; Aug. 1996

NIFS-430 R.L. Tobler, A. Nishimura and J. Yamamoto,
Design-Relevant Mechanical Properties of 316-Type Stainless Steels for Superconducting Magnets; Aug. 1996

NIFS-431 K. Tsuzuki, M. Natsir, N. Inoue, A. Sagara, N. Noda, O. Motojima, T. Mochizuki, T. Hino and T. Yamashina,
Hydrogen Absorption Behavior into Boron Films by Glow Discharges in Hydrogen and Helium; Aug. 1996

NIFS-432 T.-H. Watanabe, T. Sato and T. Hayashi,
Magnetohydrodynamic Simulation on Co- and Counter-helicity Merging of Spheromaks and Driven Magnetic Reconnection; Aug. 1996

NIFS-433 R. Horiuchi and T. Sato,
Particle Simulation Study of Collisionless Driven Reconnection in a Sheared Magnetic Field; Aug. 1996

NIFS-434 Y. Suzuki, K. Kusano and K. Nishikawa,
Three-Dimensional Simulation Study of the Magnetohydrodynamic Relaxation Process in the Solar Corona. II.; Aug. 1996

NIFS-435 H. Sugama and W. Horton,
Transport Processes and Entropy Production in Toroidally Rotating Plasmas with Electrostatic Turbulence; Aug. 1996

NIFS-436 T. Kato, E. Rachlew-Källne, P. Hörling and K.-D Zastrow,
Observations and Modelling of Line Intensity Ratios of OV Multiplet Lines for 2s3s 3S1 - 2s3p 3Pj; Aug. 1996

NIFS-437 T. Morisaki, A. Komori, R. Akiyama, H. Idei, H. Iguchi, N. Inoue, Y. Kawai, S.

Kubo, S. Masuzaki, K. Matsuoka, T. Minami, S. Morita, N. Noda, N. Ohyabu, S. Okamura, M. Osakabe, H. Suzuki, K. Tanaka, C. Takahashi, H. Yamada, I. Yamada and O. Motojima,
Experimental Study of Edge Plasma Structure in Various Discharges on Compact Helical System; Aug. 1996

NIFS-438 A. Komori, N. Ohyabu, S. Masuzaki, T. Morisaki, H. Suzuki, C. Takahashi, S. Sakakibara, K. Watanabe, T. Watanabe, T. Minami, S. Morita, K. Tanaka, S. Ohdachi, S. Kubo, N. Inoue, H. Yamada, K. Nishimura, S. Okamura, K. Matsuoka, O. Motojima, M. Fujiwara, A. Iiyoshi, C. C. Klepper, J.F. Lyon, A.C. England, D.E. Greenwood, D.K. Lee, D.R. Overbey, J.A. Rome, D.E. Schechter and C.T. Wilson,
Edge Plasma Control by a Local Island Divertor in the Compact Helical System; Sep. 1996 (IAEA-CN-64/C1-2)

NIFS-439 K. Ida, K. Kondo, K. Nagaski T. Hamada, H. Zushi, S. Hidekuma, F. Sano, T. Mizuuchi, H. Okada, S. Besshou, H. Funaba, Y. Kurimoto, K. Watanabe and T. Obiki,
Dynamics of Ion Temperature in Heliotron-E; Sep. 1996 (IAEA-CN-64/CP-5)

NIFS-440 S. Morita, H. Idei, H. Iguchi, S. Kubo, K. Matsuoka, T. Minami, S. Okamura, T. Ozaki, K. Tanaka, K. Toi, R. Akiyama, A. Ejiri, A. Fujisawa, M. Fujiwara, M. Goto, K. Ida, N. Inoue, A. Komori, R. Kumazawa, S. Masuzaki, T. Morisaki, S. Muto, K. Narihara, K. Nishimura, I. Nomura, S. Ohdachi, M.. Osakabe, A. Sagara, Y. Shirai, H. Suzuki, C. Takahashi, K. Tsumori, T. Watari, H. Yamada and I. Yamada,
A Study on Density Profile and Density Limit of NBI Plasmas in CHS; Sep. 1996 (IAEA-CN-64/CP-3)

NIFS-441 O. Kaneko, Y. Takeiri, K. Tsumori, Y. Oka, M. Osakabe, R. Akiyama, T. Kawamoto, E. Asano and T. Kuroda,
Development of Negative-Ion-Based Neutral Beam Injector for the Large Helical Device; Sep. 1996 (IAEA-CN-64/GP-9)

NIFS-442 K. Toi, K.N. Sato, Y. Hamada, S. Ohdachi, H. Sakakita, A. Nishizawa, A. Ejiri, K. Narihara, H. Kuramoto, Y. Kawasumi, S. Kubo, T. Seki, K. Kitachi, J. Xu, K. Ida, K. Kawahata, I. Nomura, K. Adachi, R. Akiyama, A. Fujisawa, J. Fujita, N. Hiraki, S. Hidekuma, S. Hirokura, H. Idei, T. Ido, H. Iguchi, K. Iwasaki, M. Isobe, O. Kaneko, Y. Kano, M. Kojima, J. Koog, R. Kumazawa, T. Kuroda, J. Li, R. Liang, T. Minami, S. Morita, K. Ohkubo, Y. Oka, S. Okajima, M. Osakabe, Y. Sakawa, M. Sasao, K. Sato, T. Shimpo, T. Shoji, H. Sugai, T. Watari, I. Yamada and K. Yamauti,
Studies of Perturbative Plasma Transport, Ice Pellet Ablation and Sawtooth Phenomena in the JIPP T-IIU Tokamak; Sep. 1996 (IAEA-CN-64/A6-5)

NIFS-443 Y. Todo, T. Sato and The Complexity Simulation Group,
Vlasov-MHD and Particle-MHD Simulations of the Toroidal Alfvén Eigenmode; Sep. 1996 (IAEA-CN-64/D2-3)

NIFS-444 A. Fujisawa, S. Kubo, H. Iguchi, H. Idei, T. Minami, H. Sanuki, K. Itoh, S. Okamura, K. Matsuoka, K. Tanaka, S. Lee, M. Kojima, T.P. Crowley, Y. Hamada, M. Iwase, H. Nagasaki, H. Suzuki, N. Inoue, R. Akiyama, M. Osakabe, S. Morita, C. Takahashi, S. Muto, A. Ejiri, K. Ida, S. Nishimura, K. Narihara, I. Yamada, K. Toi, S. Ohdachi, T. Ozaki, A. Komori, K. Nishimura, S. Hidekuma, K. Ohkubo, D.A. Rasmussen, J.B. Wilgen, M. Murakami, T. Watari and M. Fujiwara,
An Experimental Study of Plasma Confinement and Heating Efficiency through the Potential Profile Measurements with a Heavy Ion Beam Probe in the Compact Helical System; Sep. 1996 (IAEA-CN-64/C1-5)

NIFS-445 O. Motojima, N. Yanagi, S. Imagawa, K. Takahata, S. Yamada, A. Iwamoto, H. Chikaraishi, S. Kitagawa, R. Maekawa, S. Masuzaki, T. Mito, T. Morisaki, A. Nishimura, S. Sakakibara, S. Satoh, T. Satow, H. Tamura, S. Tanahashi, K. Watanabe, S. Yamaguchi, J. Yamamoto, M.Fujiwara and A. Iiyoshi,
Superconducting Magnet Design and Construction of LHD; Sep. 1996 (IAEA-CN-64/G2-4)

NIFS-446 S. Murakami, N. Nakajima, S. Okamura, M. Okamoto and U. Gasparino,
Orbit Effects of Energetic Particles on the Reachable β–Value and the Radial Electric Field in NBI and ECR Heated Heliotron Plasmas; Sep. 1996 (IAEA-CN-64/CP -6) Sep. 1996

NIFS-447 K. Yamazaki, A. Sagara, O. Motojima, M. Fujiwara, T. Amano, H. Chikaraishi, S. Imagawa, T. Muroga, N. Noda, N. Ohyabu, T. Satow, J.F. Wang, K.Y. Watanabe, J. Yamamoto , H. Yamanishi, A. Kohyama, H. Matsui, O. Mitarai, T. Noda, A.A. Shishkin, S. Tanaka and T. Terai
Design Assessment of Heliotron Reactor; Sep. 1996 (IAEA-CN-64/G1-5)

NIFS-448 M. Ozaki, T. Sato and the Complexity Simulation Group,
Interactions of Convecting Magnetic Loops and Arcades; Sep. 1996

NIFS-449 T. Aoki,
Interpolated Differential Operator (IDO) Scheme for Solving Partial Differential Equations; Sep. 1996

NIFS-450 D. Biskamp and T. Sato,
Partial Reconnection in the Sawtooth Collapse; Sep. 1996

NIFS-451 J. Li, X. Gong, L. Luo, F.X. Yin, N. Noda, B. Wan, W. Xu, X. Gao, F. Yin, J.G. Jiang, Z. Wu., J.Y. Zhao, M. Wu, S. Liu and Y. Han,
Effects of High Z Probe on Plasma Behavior in HT-6M Tokamak; Sep. 1996

NIFS-452 N. Nakajima, K. Ichiguchi, M. Okamoto and R.L. Dewar,
Ballooning Modes in Heliotrons/Torsatrons; Sep. 1996 (IAEA-CN-64/D3-6)

NIFS-453 A. Iiyoshi,
Overview of Helical Systems; Sep. 1996 (IAEA-CN-64/O1-7)

NIFS-454 S. Saito, Y. Nomura, K. Hirose and Y.H. Ichikawa,

Separatrix Reconnection and Periodic Orbit Annihilation in the Harper Map; Oct. 1996

NIFS-455 K. Ichiguchi, N. Nakajima and M. Okamoto,
Topics on MHD Equilibrium and Stability in Heliotron / Torsatron; Oct. 1996

NIFS-456 G. Kawahara, S. Kida, M. Tanaka and S. Yanase,
Wrap, Tilt and Stretch of Vorticity Lines around a Strong Straight Vortex Tube in a Simple Shear Flow; Oct. 1996

NIFS-457 K. Itoh, S.- I. Itoh, A. Fukuyama and M. Yagi,
Turbulent Transport and Structural Transition in Confined Plasmas; Oct. 1996

NIFS-458 A. Kageyama and T. Sato,
Generation Mechanism of a Dipole Field by a Magnetohydrodynamic Dynamo; Oct. 1996

NIFS-459 K. Araki, J. Mizushima and S. Yanase,
The Non-axisymmetric Instability of the Wide-Gap Spherical Couette Flow; Oct. 1996

NIFS-460 Y. Hamada, A. Fujisawa, H. Iguchi, A. Nishizawa and Y. Kawasumi,
A Tandem Parallel Plate Analyzer; Nov. 1996

NIFS-461 Y. Hamada, A. Nishizawa, Y. Kawasumi, A. Fujisawa, K. Narihara, K. Ida, A. Ejiri, S. Ohdachi, K. Kawahata, K. Toi, K. Sato, T. Seki, H. Iguchi, K. Adachi, S. Hidekuma, S.Hirokura, K. Iwasaki, T. Ido, M. Kojima, J. Koong, R. Kumazawa, H. Kuramoto, T. Minami, I. Nomura, H. Sakakita, M. Sasao, K.N. Sato, T. Tsuzuki, J. Xu, I. Yamada and T. Watari,
Density Fluctuation in JIPP T-IIU Tokamak Plasmas Measured by a Heavy Ion Beam Probe; Nov. 1996

NIFS-462 N. Katsuragawa, H. Hojo and A. Mase,
Simulation Study on Cross Polarization Scattering of Ultrashort-Pulse Electromagnetic Waves; Nov. 1996

NIFS-463 V. Voitsenya, V. Konovalov, O. Motojima, K. Narihara, M. Becker and B. Schunke,
Evaluations of Different Metals for Manufacturing Mirrors of Thomson Scattering System for the LHD Divertor Plasma; Nov. 1996

NIFS-464 M. Pereyaslavets, M. Sato, T. Shimozuma, Y. Takita, H. Idei, S. Kubo, K. Ohkubo and K. Hayashi,
Development and Simulation of RF Components for High Power Millimeter Wave Gyrotrons; Nov. 1997